Renormalization approach to the Kubo formula in Fibonacci systems

Vicenta Sánchez, Luis A. Pérez, Raúl Oviedo-Roa,* and Chumin Wang
Instituto de Investigaciones en Materiales, Universidad Nacional Autónoma de Mexico, Apartado Postal 70-360, Distrito Federal, 04510, Mexico

(Received 10 May 2001; revised manuscript received 9 July 2001; published 10 October 2001)

A renormalization method is developed for the Kubo-Greenwood formula, in order to analyze the electronic transport in large quasiperiodic lattices at zero temperature, within a tight-binding model. The results show a scaling invariance of the conduction spectrum around the transparent state, where a periodic oscillating pattern is found. However, the dc conductivity averaged over the transmission window of the leads presents a significant reduction, when the system size becomes macroscopic. A detailed study of the boundary-condition effects on the ac conductivity reveals the robustness of the transparent states, contrary to that observed in other high dc-conduction states.

DOI: 10.1103/PhysRevB.64.174205 PACS number(s): 71.23.Ft, 72.15.−v, 05.10.Cc

I. INTRODUCTION

Nowadays, with the use of modern high-speed computers, large-scale numerical calculation have been carried out to show the band structures and the eigenfunctions of thousands-atom systems. However, such computations are very time consuming and it is still difficult to address real macroscopic-scale solids. An alternate and more efficient way to achieve this is the renormalization group method, which has been quite successful in the theory of critical phenomena.[1] Recently, the real-space renormalization techniques have been applied to disordered[2,3] and quasiperiodic[4–7] systems, due to the lack of a general Bloch-type theorem for these cases. In particular, the quasiperiodic systems are highly sensitive to local defects[8] and then, it becomes essential to be able to study larger-size systems in order to minimize the boundary effects. On the other hand, the localization and transport of electrons in these systems have been a controversial issue, since the discovery of quasicrystalline alloys in 1984. At the present time, there is a consensus that the eigenvalue spectrum produced by a quasiperiodic potential is singular continuous and the associated eigenfunctions are critical.[9] Moreover, the level-spacing statistics show an inverse-power-law distribution of gaps[10,11] and a semi-Poisson distribution of bands,[12] both neither conventional Poisson nor Wigner ones. Hence, the electrical conduction of these critically localized states becomes an especially interesting subject. The hopping conductivity in Fibonacci chains has been addressed by using the Miller-Abrahams equations[13,14] and the optical conductivity has been analyzed within a generalized Drude formula.[15] Recently, *transparent states* with unity transmission coefficient have been reported for mixing Fibonacci systems of N atoms.[16] It is observed that the eigenfunctions of these transparent states, with energies satisfying $E=\alpha(1+\gamma^2)/(1-\gamma^2)$ and $E^2-\alpha^2=4t^2\cos^2(K\pi/N)$, are periodiclike wave functions,[17] where $+\alpha$ $(-\alpha)$ are the on-site energies of atoms A (B), $\gamma=t_{AA}/t_{AB}$ is the ratio of the hopping parameters, and K and N/K are integer numbers. Furthermore, the ac conductivity of these transparent states has been analyzed within the Kubo-Greenwood formalism,[18] which has the advantage of allowing the analysis of transport in any dimensional systems at finite electric-field frequency and finite temperature. In this paper, we report a renormalization method for the Kubo-Greenwood formula and scale invariances of the dc and ac conductivities around the transparent states in mixing Fibonacci chains.

This paper is organized as follows. Section II defines the system and introduces the renormalization method. The mathematical details of the method are given in the Appendixes. In Sec. III, the dc conductivity is analyzed for different quasiperiodic-system sizes and its behavior around the transparent state is investigated in detail. In Sec. IV, the ac conductivities calculated by using free, finite-lead and almost-infinite-lead boundary conditions are reported. In particular, the low-frequency behaviors for the transparent and non transparent states are comparatively shown. Finally, the conclusions are given in Sec. V.

II. THE RENORMALIZATION METHOD

In a mixing Fibonacci system (MFS) two kinds of atoms, A and B, are arranged following the Fibonacci sequence and the hopping integrals between the atoms depends on the nature of them, giving rise to the existence of two different parameters t_{AA} and $t_{AB}=t_{BA}$.[16] In this paper, we define the first generation $F_1=A$ and the second generation $F_2=BA$. The next generations are given by $F_n=F_{n-1}\oplus F_{n-2}$, containing $N(n)$ atoms. For the sake of simplicity, an uniform bond length (a) is taken. Moreover, in order to isolate the quasicrystalline effects on the physical properties of the system, a simple s-band tight-binding Hamiltonian is considered as given in Ref. 18. The analysis of the electrical conductivity is carried out by using the Kubo-Greenwood formula, which can be written as[19]

$$\sigma(\mu,\omega,T)=\lim_{\Omega\to\infty}\frac{2e^2\hbar}{\pi\Omega m^2}\int_{-\infty}^{\infty}dE\,\frac{f(E)-f(E+\hbar\omega)}{\hbar\omega}\times\mathrm{Tr}[p\,\mathrm{Im}\,G^{+}(E+\hbar\omega)p\,\mathrm{Im}\,G^{+}(E)],\quad(1)$$

where Ω is the volume of the system, $p=(ima/\hbar)\Sigma_j\{t_{j,j+1}|j\rangle\langle j+1|-t_{j,j-1}|j\rangle\langle j-1|\}$ is the projection of the momentum operator along the applied electric-

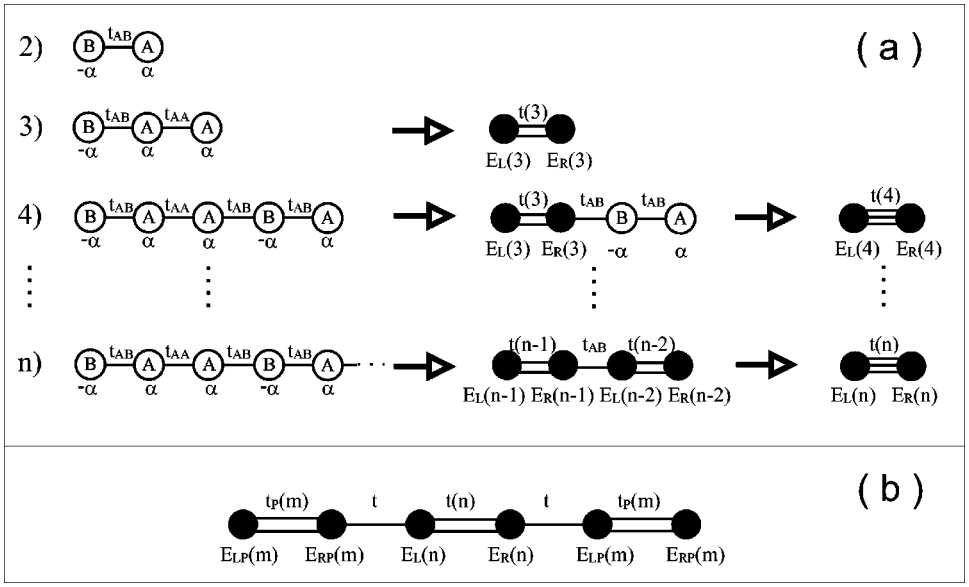

FIG. 1. (a) Schematic representation of the renormalization procedure. The numbers on the left side indicate the generation. The nature of atoms, their self-energies, and the hopping parameters are specified inside, below, and between the open circles, respectively. At the end of the process one gets two effective atoms (black circles) with a single effective bond. There is an intermediate step in which renormalized chains of lower generations are connected together through a hopping t_{AB}. (b) Sketch of an MFS of generation n connected to two periodic leads through the same hopping t of the periodic leads.

field direction, $G^+(E)$ is the retarded one-particle Green's function, and $f(E)=\{1+\exp[(E-\mu)/k_BT]\}^{-1}$ is the Fermi-Dirac distribution with Fermi energy μ and temperature T.

For an infinite periodic linear chain with null self-energies and hopping integral t, the conductivity of a segment of N atoms at zero temperature can be calculated analytically and it is given by[20]

$$\sigma(\mu=0,\omega)=\frac{8e^2t^2a}{\pi(N-1)\hbar^3\omega^2}\left\{1-\cos\left[(N-1)\frac{\hbar\omega}{2|t|}\right]\right\}, \tag{2}$$

where the system length is $\Omega=(N-1)a$. In the limit of $\omega\to0$, the dc conductivity within the energy band is

$$\sigma_p=\frac{e^2a}{\pi\hbar}(N-1). \tag{3}$$

This yields a finite conductance $g\equiv\sigma_p/(N-1)a=2e^2/h$, which has been observed recently.[21]

For quasiperiodic systems, however, in spite of the wide use of the renormalization group (RG) methods in their study, the electrical conductivity in these systems has not been explored in that way, due to the complex processes involved in transport phenomena. Following the RG scheme shown in Fig. 1(a), we have found an iterative procedure to calculate directly the product of the Green's function involved in the Kubo-Greenwood formula [Eq. (1)], which can be written conveniently for a finite MFS of generation n at $T=0$ as

$$\sigma(\mu,\omega)=-\frac{2e^2a^2}{\pi\Omega\hbar^2\omega}\int_{\mu-\hbar\omega}^{\mu}dE\sum_{j,k=1}^{N(n)-1}t_{j,j+1}t_{k,k+1}[2\,\mathrm{Im}\,G^+_{j+1,k}(E_\omega,n)\mathrm{Im}\,G^+_{k+1,j}(E,n)-\mathrm{Im}\,G^+_{j+1,k+1}(E_\omega,n)\mathrm{Im}\,G^+_{k,j}(E,n)$$
$$-\mathrm{Im}\,G^+_{j,k}(E_\omega,n)\mathrm{Im}\,G^+_{k+1,j+1}(E,n)]=\frac{e^2a^2}{2\pi\Omega\hbar^2\omega}\int_{\mu-\hbar\omega}^{\mu}dE[S(E^+_\omega,E^+,n)-S(E^+_\omega,E^-,n)-S(E^-_\omega,E^+,n)$$
$$+S(E^-_\omega,E^-,n)], \tag{4}$$

where $E^\pm=E\pm i\delta$, $E_\omega=E+\hbar\omega$, and then $E^\pm_\omega=E+\hbar\omega\pm i\delta$ with $\delta\to0$. Furthermore, the symmetry $G_{j,k}=G_{k,j}$ and the relationship $\mathrm{Im}\,G^+=(G^+-G^-)/2i$ have been used, since $G^\pm(E)=G(E^\pm)$ and the eigenfunctions are real for finite systems. In Eq. (4) the partial sums $S(E^\nu_\omega,E^\beta,n)$ are defined as

$$S(E^\nu_\omega,E^\beta,n)=\sum_{j,k=1}^{N(n)-1}t_{j,j+1}t_{k,k+1}[2G_{j+1,k}(E^\nu_\omega)G_{k+1,j}(E^\beta)-G_{j+1,k+1}(E^\nu_\omega)G_{k,j}(E^\beta)-G_{j,k}(E^\nu_\omega)G_{k+1,j+1}(E^\beta)], \tag{5}$$

where ν and β can be either $+$ or $-$. These partial sums can be expressed in terms of the Green's functions at the extreme sites of the MFS as

$$S(E_\omega^\nu,E^\beta,n)=A(E_\omega^\nu,E^\beta,n)G_{L,L}(E_\omega^\nu)G_{L,L}(E^\beta)+B(E_\omega^\nu,E^\beta,n)G_{L,R}(E_\omega^\nu)G_{L,R}(E^\beta)+C(E_\omega^\nu,E^\beta,n)G_{R,R}(E_\omega^\nu)G_{R,R}(E^\beta)$$
$$+D(E_\omega^\nu,E^\beta,n)G_{L,L}(E_\omega^\nu)G_{L,R}(E^\beta)+D(E^\beta,E_\omega^\nu,n)G_{L,L}(E^\beta)G_{L,R}(E_\omega^\nu)+F(E_\omega^\nu,E^\beta,n)G_{L,L}(E_\omega^\nu)G_{R,R}(E^\beta)$$
$$+F(E^\beta,E_\omega^\nu,n)G_{L,L}(E^\beta)G_{R,R}(E_\omega^\nu)+I(E_\omega^\nu,E^\beta,n)G_{L,R}(E_\omega^\nu)G_{R,R}(E^\beta)+I(E^\beta,E_\omega^\nu,n)G_{L,R}(E^\beta)G_{R,R}(E_\omega^\nu)$$
$$+J(E_\omega^\nu,E^\beta,n)G_{L,L}(E_\omega^\nu)+J(E^\beta,E_\omega^\nu,n)G_{L,L}(E^\beta)+K(E_\omega^\nu,E^\beta,n)G_{L,R}(E_\omega^\nu)+K(E^\beta,E_\omega^\nu,n)G_{L,R}(E^\beta)$$
$$+L(E_\omega^\nu,E^\beta,n)G_{R,R}(E_\omega^\nu)+L(E^\beta,E_\omega^\nu,n)G_{R,R}(E^\beta)+Z(E_\omega^\nu,E^\beta,n), \quad (6)$$

where the subindexes L and R denote the left- and the right-end atoms, respectively. The coefficients $A(E_1,E_2,n)$, $B(E_1,E_2,n)$, . . . , $Z(E_1,E_2,n)$ in the last equation, being E_1 and E_2 either E_ω^ν or E^β, can be iteratively obtained from those of generations $n-1$ and $n-2$, as shown in Appendix A and the detail of the calculation is given in Appendix B.

For the free-boundary condition, the Green's functions $G_{L,L}$, $G_{R,R}$, and $G_{L,R}$ are determined by solving a two-site Dyson equation. In the case of finite periodic leads, the MFS and the leads can be renormalized to two effective site systems each one and then, a six-site Dyson equation should be solved as shown in Fig. 1(b). The leads and the MFS are connected by the same hopping parameter of the periodic leads. Finally, for the almost-infinite-periodic-lead case, with more than 10^{20} atoms in each lead, we have to solve only a four-site Dyson equation since the renormalized hopping integral of the leads becomes essentially zero. On the other hand, the total density of states can be also calculated by means of a similar renormalization procedure as shown in Eq. (A1) of Appendix A. In the next section, we use this method to analyze the dc conductivity of MFS for a wide range of system sizes.

III. SIZE SCALING BEHAVIOR

Let us consider a MFS with $k\equiv N/K=4$, as defined in Ref. 17, connected to two almost-infinite periodic linear chains (leads) with hopping integrals t and null on-site energies, where almost-infinite means large enough so that the physical quantities have no important variation with the lead size. The trace in Eq. (1) is taken over the MFS. The numerical results of finite MFS with $k=2$ and $k=3$ have been studied in Ref. 18. Figures 2(a) and 2(b) show respectively the normalized density of states (DOS/N) and the normalized zero-temperature dc Kubo conductivity ($\sigma(\mu,0)/\sigma_P$), both in logarithmic scale, of a MFS with $\alpha=0.5|t|$, $\gamma=\sqrt{2}$ and $n=41$. The spectra contain 10^5 data and have been calculated in quadruple precision. The imaginary part of the energy in the Green's function is $\delta=10^{-11}|t|$ and the transparent state energy ($E_T=-1.5|t|$) is indicated by a dashed line. Notice first that the considered MFS contains 267 914 296 atoms ($n=41$), hence the multifractal band structure is quite fine, and in consequence a finite number grid can not show the whole feature of the spectrum. Such is the case for the dc conductivity spectrum around $\mu=1.4|t|$, since the conduction minibands are sharper than those of the DOS as occurs in disordered systems.[22] On the other hand, it is observed that around the transparent state both spectra have an almost constant behavior, as analyzed in the following.

Figures 3(a) and 3(b) show, respectively, amplifications of the DOS and of the Kubo dc conductivity around the transparent state, for generations $n=6l-1$ (open circles); $6l$, $6l+1$, $6l-2$ (black line); $6l+2$ (gray line); and $6l+3$ (light gray line), being $l=1,2,3,\ldots$. Notice first that periodic oscillating behaviors with the same energy period given approximately by $\Delta=4.546|t|/(N-1)$ are present in both amplified spectra. The dc conductivity spectrum can be reproduced reasonably well by evaluating the transmittance of the MFS.[18] For $\mu=E_T$, the transfer matrices commute and the transmittance (τ) is given by[16]

$$\tau(\mu,N)=\left[1+\frac{(1-\gamma^2)^2\sin^2(N\phi)}{(4-(\mu/t)^2)\gamma^2}\right]^{-1}, \quad (7)$$

where $2|t|\cos\phi=\sqrt{\mu^2-\alpha^2}$, as shown in Fig. 3(c). For energies very close to E_T, considering that $N\gg 1$, their transfer matrices almost commute. Hence, a slight difference between Figs. 3(b) and 3(c) is observed. The general oscillating behavior for any generation can be explained by considering

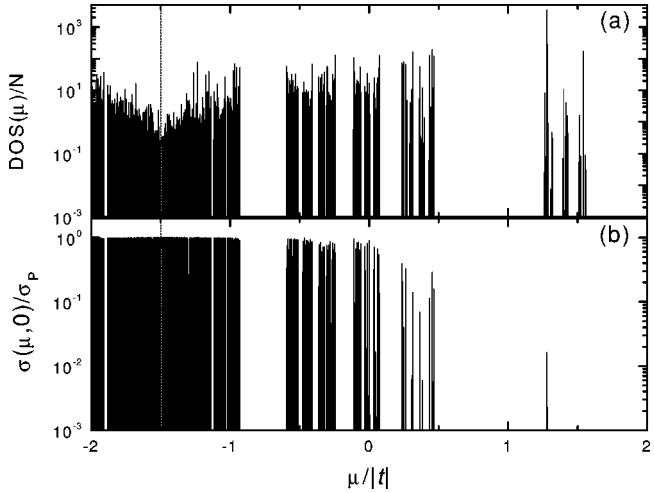

FIG. 2. (a) Density of states (DOS), and (b) the normalized Kubo dc conductivity [$\sigma(\mu,0)/\sigma_P$] for a mixing Fibonacci system (MFS) of generation $n=41$ with $k=4$, $\alpha=0.5|t|$ and $\gamma=\sqrt{2}$, connected to two 10^{20}-atom periodic linear chains with $\alpha=0$ and hopping integral t. Both spectra contain 10^5 data and Im(E) $=10^{-11}|t|$. The transparent state ($E_T=-1.5|t|$) is indicated by a dashed line.

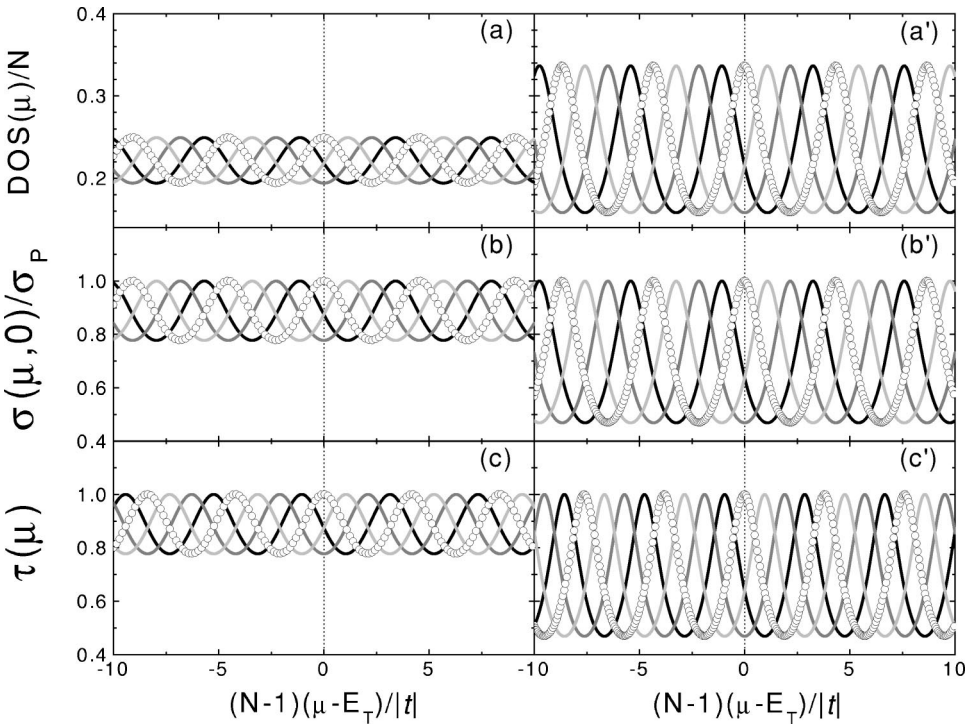

FIG. 3. Amplifications of (a) the density of states (DOS) and (b) the Kubo dc conductivity (σ) around the transparent state, for generations $n=6l-1$ (open circles); $6l$, $6l+1$, $6l-2$ (black line); $6l+2$ (gray line); and $6l+3$ (light gray line), for a MFS with the same Hamiltonian parameters as in Fig. 2, l being a large integer number. These spectra are compared with that obtained by evaluating Eq. (7) and shown in (c). The corresponding spectra for an MFS with $\alpha=0.85|t|$, $\gamma=1.25\sqrt{2}$, and $E_T=-1.65|t|$, are shown in figures (a′), (b′), and (c′).

that $N\phi(E_T)=K\pi+(r/k)\pi$, $(\mu-E_T)/|t|\ll 1$, and $\phi(\mu)-\phi(E_T)\ll 1$, being $r=0,1,2,\ldots,k-1$ and $N=Kk+r$. Thus,

$$\cos\phi(\mu)\simeq\cos\phi(E_T)-[\phi(\mu)-\phi(E_T)]\sin\phi(E_T)$$

and

$$\frac{\sqrt{\mu^2-\alpha^2}}{2|t|}\simeq\frac{\sqrt{E_T^2-\alpha^2}}{2|t|}\left(1+2\frac{|t|E_T}{E_T^2-\alpha^2}\frac{(\mu-E_T)}{|t|}\right).$$

Therefore, the definition of $\phi(\mu)$, $2|t|\cos\phi(\mu)=\sqrt{\mu^2-\alpha^2}$, leads to

$$\phi(\mu)-\phi(E_T)\simeq-\frac{E_T}{4|t|\sin\phi(E_T)\cos\phi(E_T)}\frac{(\mu-E_T)}{|t|}=\Lambda\frac{(\mu-E_T)}{|t|},$$

where $\Lambda\equiv-E_T/\{2|t|\sin[2\phi(E_T)]\}$. In consequence, for $N\to\infty$,

$$\tau(\mu,N)\to\left[1+\frac{(1-\gamma^2)^2\sin^2\left[\Lambda\varepsilon+\frac{r}{k}\pi\right]}{[4-(E_T/t)^2]\gamma^2}\right]^{-1},$$

where $\varepsilon\equiv N(\mu-E_T)/|t|$ and μ in the denominator of Eq. (7) has been replaced by E_T, because $(\mu-E_T)/|t|\ll 1$. Notice that the transmittance, or the conductivity, is an oscillating function of ε and size scaling invariant in the neighborhood of the transparent state. The phase of this oscillation is determined by r. For the case $k=4$, $\phi(E_T)=\pi/4$. Hence, for generations $n=6l-1$, $N(n)$ is multiple of 4 and then $r=0$; for $n=6l$, $6l+1$, and $6l-2$, $r=1$; for $n=6l+2$, $r=2$; and finally, for $n=6l+3$, $r=3$.

Furthermore, the amplitude of these periodic oscillations increases when the chemical diversity parameter (α) of the system grows. This feature is shown in Figs. 3(a′), 3(b′), and 3(c′), for a MFS with $\alpha=0.85|t|$, $\gamma=1.25\sqrt{2}$, and $E_T=-1.65|t|$. It is important to stress that the spectra around the transparent states are scale invariant even though the whole spectra is not.

In order to analyze the global dc conduction properties of the system, we introduce the lead-transmission-window-averaged dc conductivity

$$\langle\sigma(\mu,0)\rangle=\frac{1}{N_\mu}\sum_{j=1}^{N_\mu}\sigma(\mu_j,0), \tag{8}$$

where μ_j are uniformly chosen from the interval $[-2|t|,2|t|]$, which corresponds to the transmission window of the periodic leads. The number of energies contributing significantly to this average can be quantified by using the conductivity participation ratio (CPR) defined by

$$\mathrm{CPR}=\frac{\left[\sum_{j=1}^{N_\mu}\sigma^2(\mu_j,0)\right]^2}{N_\mu\sum_{j=1}^{N_\mu}\sigma^4(\mu_j,0)}. \tag{9}$$

In Figs. 4(a), 4(b), and 4(c), the transmission-window-averaged dc conductivity [$\langle\sigma(\mu,0)\rangle$], the conductivity participation ratio (CPR) and the transparent-energy conductivity [$\sigma(E_T,0)$] are respectively plotted as a function of the system size for $N_\mu=10^5$ and the same MFS as in Fig. 2.

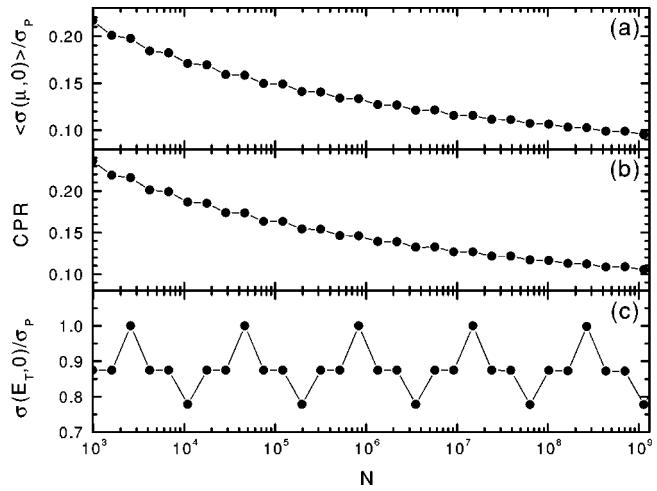

FIG. 4. (a) Lead-transmission-window-averaged dc conductivity ($\langle\sigma(\mu,0)\rangle$), (b) conductivity participation ratio (CPR), and (c) transparent-energy conductivity $[\sigma(E_T,0)]$ as a function of the system size for the same MFS as Fig. 2 and $N_\mu=10^5$.

Notice the clear decay of the averaged conductivity, which can be related to the opening of gaps when the MFS grows. This possible reason has been confirmed by the CPR. In contrast to the monotonously decay behavior, the dc conductivity evaluated at the transparent state energy ($E_T=-1.5|t|$) oscillates periodically, because for MFS with $k=4$ the system has an unity transmission coefficient each six generations, since $k=4$ is divisor of N for generations $n=6l-1$, with $l=1,2,3,\ldots$.[17] The oscillating behavior of the normalized dc conductivity shown in Fig. 4(c) is confirmed by Eq. (7), since the dc conductivity is proportional to the transmittance through Landauer formula and it is in very good agreement with that calculated by means of Kubo-Greenwood formula.[18] In the next section, the ac conductivity and its sensitivity to boundary conditions are investigated.

IV. BOUNDARY CONDITION ANALYSIS

In Fig. 5, the ac Kubo conductivity of the transparent state is shown for three MFS with the same self-energies and hopping integrals as in Fig. 2, but different boundary conditions, i.e., (a′) 4 807 526 976 atoms without leads, (b′) 267 914 296 atoms connected to two 2 269 806 340 atom periodic linear chains, and (c′) 267914296 atoms saturated by two periodic linear chains of 10^{20} atoms. Figures 5(a), 5(b), and 5(c) show the results obtained for a periodic system with $\mu=0$, and the same lengths and boundary conditions as in Figs. 5(a′), 5(b′), and 5(c′), respectively. The ac conductivities are calculated by using $\mathrm{Im}(E)=10^{-11}|t|$. Observe that in Figs. 5(a) and 5(b) the systems including the leads have an equal total number of atoms; therefore, the resonance peaks are located at the same frequencies, since the eigenvalue spectra are the same and the resonance peaks are determined by the Fermi-golden selection rules.[23] However, their amplitudes are very different, because the Kubo formula is evaluated on different system lengths. Furthermore, the minima of Figs. 5(b) and 5(c) seem to be located at the same values of frequency, except that in Fig. 5(c) a continuous behavior is observed due to the presence of almost-infinite leads. For the latter case, the ac conductivity is given by Eq. (2). All these features are mainly preserved for the transparent states as shown in Figs. 5(a′), 5(b′), and 5(c′), except for a compression of the spectra due to the presence of gaps in the Fibonacci eigenvalue spectrum.

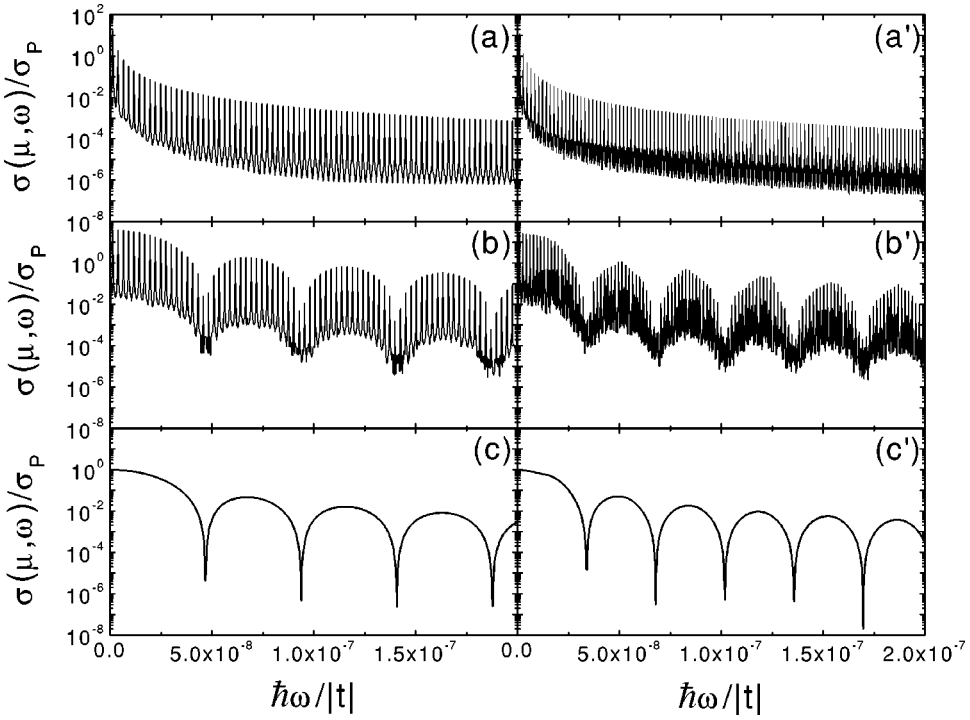

FIG. 5. ac Kubo conductivity of the transparent state ($\mu=E_T$) for three MFS with the same self-energies and hopping integrals as in Fig. 2, but different boundary conditions, i.e., (a′) 4 807 526 976 atoms ($n=47$) without leads, (b′) 267 914 296 atoms ($n=41$) connected to two 2 269 806 340-atom periodic linear chains, and (c′) 267 914 296 atoms saturated by two periodic leads of 10^{20} atoms. Figures (a), (b), and (c) show the corresponding results obtained for a periodic system with $\mu=0$.

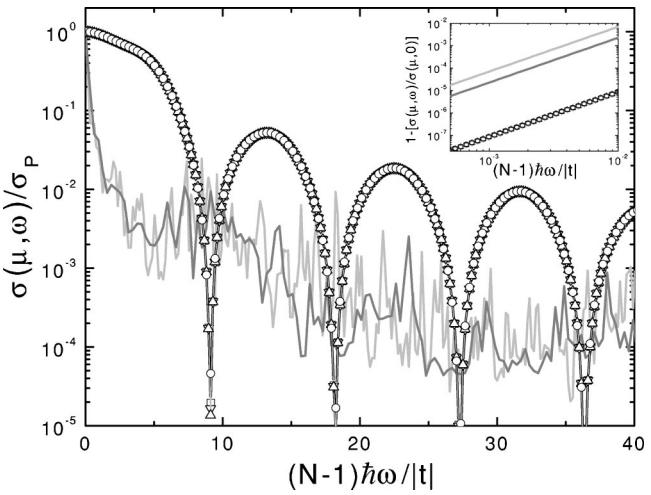

FIG. 6. ac Kubo conductivity for the same MFS as in Fig. 2 but with $n=6l$, $6l+1$, $6l+4$ (up triangles), $n=6l+2$ (down triangles), and $n=6l+3$ (open squares), evaluated at $\mu=E_T-\Delta/4$, $E_T-\Delta/2$, and $E_T-3\Delta/4$, respectively, in comparison with that of the transparent state (open circles), where $\Delta=4.546|t|/(N-1)$. The non-transparent-state ac conductivities with $\mu_1=-0.591\,763\,398|t|$ (gray line) and $\mu_2=-0.108\,600\,000\,01|t|$ (light gray line) are also shown. In the inset a low-frequency-regime log-log plot of the ac conductivity is presented.

In Fig. 6, the ac Kubo conductivity of two kinds of non-transparent states are shown in comparison with that of the transparent state (open circles) for the same MFS as in Fig. 2. First, for generations $n=6l$, $6l+1$, and $6l+4$ (up triangles), $n=6l+2$ (down triangles), and $n=6l+3$ (open squares), the ac conductivity is evaluated at their maximum dc-conductivity energies [see Fig. 3(a)] located at $\mu=E_T-\Delta/4$, $E_T-\Delta/2$, and $E_T-3\Delta/4$, respectively. Notice that these almost-transparent states have the same frequency dependence except that the initial value at $\omega=0$ is strictly unity only for the transparent state of generation $n=6l+5$. It is important to mention that these curves are scale invariant, which is related to the scaling invariance shown in Fig. 3, since the zero-temperature ac conductivity is calculated by integrating a vicinity of $\hbar\omega$ around the Fermi energy [Eq. (1)]. For the second kind of nontransparent states, i.e., high dc conductivity states with $\mu\neq E_T$ in the same MFS of generation 41 as in Fig. 2, a noisy behavior is observed for $\mu_1=-0.591\,763\,398|t|$ (gray line) and $\mu_2=-0.108\,600\,000\,01|t|$ (light gray line), with $\sigma(\mu_1,0)/\sigma_P=0.9701$ and $\sigma(\mu_2,0)/\sigma_P=0.95$. It is important to stress that these ac conductivities are not scale invariant, and decay with the frequency much faster than that of the transparent ones, since the ac conductivity depends not only on the states at the Fermi level but also on the localization condition of the states in a range of $\hbar\omega$ around it.

A log-log plot of the ac conductivity in the low-frequency limit is shown in the inset of Fig. 6, where the calculations were performed using $\mathrm{Im}(E)=10^{-15}|t|$. Observe that the transparent state and the almost-transparent states have the same conductivity in the low-frequency limit, which follows essentially the same relationship as the periodic case with $\mu=0$,[20]

$$\sigma(0,\omega)=\frac{e^2a(N-1)}{\pi\hbar}\left\{1-\frac{1}{48}\left[\frac{(N-1)\hbar\omega}{2|t|}\right]^2\right\}, \quad (10)$$

except for the coefficient of 0.084 84, instead of 1/48; while the coefficients are 22.3934 and 69.0557 for the nontransparent states with μ_1 and μ_2, respectively. Note that the larger coefficients of the nontransparent states confirm the dramatic decay of their ac conductivity when an oscillating electrical field is turned on.

V. CONCLUSIONS

In summary, we have developed a renormalization procedure for evaluating the Kubo-Greenwood formula in Fibonacci lattices, which allows the study of the electrical transport in macroscopic quasiperiodic systems. In particular, we have analyzed the dc and ac conductivity at zero temperature in MFS. The results show a *scale invariance* of the dc conduction spectrum around the transparent state, where a periodic oscillating pattern is found. The amplitude of these oscillations increase when the inhomogeneity or chemical diversity of the system grows. Furthermore, a significant reduction of the transmission-window-averaged dc conductivity is observed when the MFS grows, fact related to the multifractal band fragmentation,[24] which is confirmed by quantifying the number of participating states to the averaged conductivity.

The ac conduction analysis reveals that in spite of a general conductivity diminution as the frequency of the applied field increases, the transparent and almost-transparent states show the same regular oscillating behavior, which is highly sensitive to the boundary conditions: (1) for the case without leads the ac conductivity decreases monotonically; (2) with finite leads an oscillatory decreasing behavior is found; (3) when almost-infinite leads are introduced the ac conductivity becomes a smooth oscillating function of the frequency, where the results have been confirmed analytically for the periodic case. In particular, for the almost-infinite lead case, a *scale invariance* of the ac conductivity is observed for the transparent and almost-transparent states. On the other hand, the diminution of the non-transparent-states ac conductivity is much faster than that of transparent ones and do not show a regular oscillating pattern. However, in the low-frequency limit they also obey the square decay rule as in periodic systems.

This renormalization method can be used to analyze the electrical transport in quasiperiodic superlattices by introducing a two-dimensional **k** space, which takes advantage of the translational symmetry in the parallel planes, as in the study of the Raman scattering in Fibonacci superlattices.[25] This work is currently in progress.

ACKNOWLEDGMENTS

This work has been partially supported by CONACyT-32148E, DGAPA-IN105999 and IN101701. Computations were performed at Origin2000 of DGSCA, UNAM.

APPENDIX A: RENORMALIZATION FORMULAS

As discussed in Sec. II, the Kubo-Greenwood conductivity can be written in terms of the partial sums, $S(E_\omega^\nu,E^\beta,n)$, defined in Eq. (5). These partial sums can be expressed as a quadratic polynomial of the Green's functions evaluated at the extreme sites of the system, as shown in Eq. (6), where the coefficients are iteratively given by

$$A(E_1,E_2,n)=-[A_c(E_1,E_2,n)-A_c(E_2,E_1,n)]^2,$$

$$B(E_1,E_2,n)=2[A_c(E_1,E_2,n)-A_c(E_2,E_1,n)][B_c(E_2,E_1,n)-B_c(E_1,E_2,n)]+2[C_c(E_1,E_2,n)-D_c(E_2,E_1,n)]\times[C_c(E_2,E_1,n)-D_c(E_1,E_2,n)],$$

$$C(E_1,E_2,n)=-[B_c(E_1,E_2,n)-B_c(E_2,E_1,n)]^2,$$

$$D(E_1,E_2,n)=2[A_c(E_1,E_2,n)-A_c(E_2,E_1,n)][D_c(E_2,E_1,n)-C_c(E_1,E_2,n)],$$

$$F(E_1,E_2,n)=-[C_c(E_1,E_2,n)-D_c(E_2,E_1,n)]^2,$$

$$I(E_1,E_2,n)=2[B_c(E_1,E_2,n)-B_c(E_2,E_1,n)][D_c(E_2,E_1,n)-C_c(E_1,E_2,n)],$$

$$\begin{aligned}J(E_1,E_2,n)=&J(E_1,E_2,n-1)+\eta_1^2(E_1,n)[\theta_2(E_2,n)C(E_1,E_2,n-1)+L(E_1,E_2,n-1)]\\&+\eta_1(E_1,n)[\theta_2(E_2,n)I(E_1,E_2,n-1)+K(E_1,E_2,n-1)+V_u(E_1,E_2,n)]+\kappa_1^2(E_1,n)[\theta_1(E_2,n)\\&\times A(E_1,E_2,n-2)+J(E_1,E_2,n-2)]+\theta_2(E_2,n)F(E_1,E_2,n-1)+\kappa_1(E_1,n)\\&\times[\eta_1(E_1,n)\theta_3(E_2,n)A_o(E_1,E_2,n)\\&+\theta_3(E_2,n)B_o(E_2,E_1,n)+W_u(E_2,E_1,n)],\end{aligned}$$

$$\begin{aligned}K(E_1,E_2,n)=&\theta_2(E_2,n)\kappa_2(E_1,n)[2\eta_1(E_1,n)C(E_1,E_2,n-1)+I(E_1,E_2,n-1)]+\kappa_2(E_1,n)[2\eta_1(E_1,n)L(E_1,E_2,n-1)\\&+K(E_1,E_2,n-1)+V_u(E_1,E_2,n)]+\theta_1(E_2,n)\kappa_1(E_1,n)[2\eta_2(E_1,n)A(E_1,E_2,n-2)+D(E_2,E_1,n-2)]\\&+\kappa_1(E_1,n)[2\eta_2(E_1,n)J(E_1,E_2,n-2)+K(E_1,E_2,n-2)+Y_u(E_2,E_1,n)]+\eta_2(E_1,n)\\&\times[\theta_3(E_2,n)B_o(E_2,E_1,n)+W_u(E_2,E_1,n)]+\eta_1(E_1,n)[\theta_3(E_2,n)D_o(E_1,E_2,n)+X_u(E_1,E_2,n)]+\theta_3(E_2,n)\\&\times\{[\kappa_2(E_1,n)\kappa_1(E_1,n)+\eta_2(E_1,n)\eta_1(E_1,n)]A_o(E_1,E_2,n)+C_o(E_2,E_1,n)\},\end{aligned}$$

$$\begin{aligned}L(E_1,E_2,n)=&L(E_1,E_2,n-2)+\eta_2^2(E_1,n)[\theta_1(E_2,n)A(E_1,E_2,n-2)+J(E_1,E_2,n-2)]+\eta_2(E_1,n)[\theta_1(E_2,n)\\&\times D(E_2,E_1,n-2)+K(E_1,E_2,n-2)+Y_u(E_2,E_1,n)]+\kappa_2^2(E_1,n)[\theta_2(E_2,n)C(E_1,E_2,n-1)\\&+L(E_1,E_2,n-1)]+\theta_1(E_2,n)F(E_2,E_1,n-2)+\kappa_2(E_1,n)[\eta_2(E_1,n)\theta_3(E_2,n)A_o(E_1,E_2,n)\\&+\theta_3(E_2,n)D_o(E_1,E_2,n)+X_u(E_1,E_2,n)],\end{aligned}$$

$$\begin{aligned}Z(E_1,E_2,n)=&Z(E_1,E_2,n-1)+Z(E_1,E_2,n-2)+\theta_1(E_1,n)[\theta_1(E_2,n)A(E_1,E_2,n-2)+J(E_1,E_2,n-2)]+\theta_2(E_1,n)\\&\times[\theta_2(E_2,n)C(E_1,E_2,n-1)+L(E_1,E_2,n-1)]+\theta_1(E_2,n)J(E_2,E_1,n-2)+\theta_2(E_2,n)L(E_2,E_1,n-1)\\&+\theta_3(E_1,n)\theta_3(E_2,n)A_o(E_1,E_2,n)+Z_u(E_1,E_2,n)+Z_u(E_2,E_1,n),\end{aligned}$$

where E_1 and E_2 can be either E_ω^ν or E^β, and

$$\theta_1(E,n)=[E-E_R(E,n-1)]/\gamma_F(E,n),$$

$$\theta_2(E,n)=[E-E_L(E,n-2)]/\gamma_F(E,n),$$

$$\theta_3(E,n)=t_{AB}/\gamma_F(E,n),\gamma_F(E,n)=[E-E_R(E,n-1)][E-E_L(E,n-2)]-t_{AB}^2,$$

$$\kappa_1(E,n)=t(E,n-1)\theta_3(E,n),\kappa_2(E,n)=t(E,n-2)\theta_3(E,n),$$

$$\eta_1(E,n)=t(E,n-1)\theta_2(E,n),\eta_2(E,n)=t(E,n-2)\theta_1(E,n),$$

$$A_c(E_1,E_2,n)=A_c(E_1,E_2,n-1)+\kappa_1(E_1,n)\kappa_1(E_2,n)A_c(E_1,E_2,n-2)+\eta_1(E_1,n)\eta_1(E_2,n)B_c(E_1,E_2,n-1)$$
$$+\eta_1(E_2,n)C_c(E_1,E_2,n-1)+\eta_1(E_1,n)D_c(E_1,E_2,n-1)+t_{AB}\kappa_1(E_1,n)\eta_1(E_2,n),$$

$$B_c(E_1,E_2,n)=B_c(E_1,E_2,n-2)+\eta_2(E_1,n)\eta_2(E_2,n)A_c(E_1,E_2,n-2)+\kappa_2(E_1,n)\kappa_2(E_2,n)B_c(E_1,E_2,n-1)$$
$$+\eta_2(E_1,n)C_c(E_1,E_2,n-2)+\eta_2(E_2,n)D_c(E_1,E_2,n-2)+t_{AB}\kappa_2(E_2,n)\eta_2(E_1,n),$$

$$C_c(E_1,E_2,n)=\kappa_1(E_1,n)\eta_2(E_2,n)A_c(E_1,E_2,n-2)+\eta_1(E_1,n)\kappa_2(E_2,n)B_c(E_1,E_2,n-1)+\kappa_2(E_2,n)C_c(E_1,E_2,n-1)$$
$$+\kappa_1(E_1,n)C_c(E_1,E_2,n-2)+t_{AB}\kappa_2(E_2,n)\kappa_1(E_1,n),$$

$$D_c(E_1,E_2,n)=\kappa_1(E_2,n)\eta_2(E_1,n)A_c(E_1,E_2,n-2)+\eta_1(E_2,n)\kappa_2(E_1,n)B_c(E_1,E_2,n-1)+\kappa_2(E_1,n)D_c(E_1,E_2,n-1)$$
$$+\kappa_1(E_2,n)D_c(E_1,E_2,n-2)+t_{AB}\eta_1(E_2,n)\eta_2(E_1,n),$$

$$V_u(E_1,E_2,n)=2t_{AB}\{\kappa_1(E_1,n)\theta_1(E_2,n)[A_c(E_1,E_2,n-2)-A_c(E_2,E_1,n-2)]+\eta_1(E_1,n)\theta_3(E_2,n)[B_c(E_1,E_2,n-1)$$
$$-B_c(E_2,E_1,n-1)]+\theta_3(E_2,n)[C_c(E_1,E_2,n-1)-D_c(E_2,E_1,n-1)]++0.5t_{AB}[\kappa_1(E_1,n)\theta_3(E_2,n)$$
$$-\eta_1(E_1,n)\theta_1(E_2,n)]\},$$

$$W_u(E_1,E_2,n)=2t_{AB}\{\theta_2(E_1,n)\eta_1(E_2,n)[B_c(E_1,E_2,n-1)-B_c(E_2,E_1,n-1)]+\theta_2(E_1,n)[D_c(E_1,E_2,n-1)$$
$$-C_c(E_2,E_1,n-1)]+0.5t_{AB}[\eta_1(E_2,n)\theta_3(E_1,n)-\theta_2(E_1,n)\kappa_1(E_2,n)]$$
$$+\theta_3(E_1,n)\kappa_1(E_2,n)[A_c(E_1,E_2,n-2)-A_c(E_2,E_1,n-2)]\},$$

$$X_u(E_1,E_2,n)=2t_{AB}\{\eta_2(E_1,n)\theta_1(E_2,n)[A_c(E_1,E_2,n-2)-A_c(E_2,E_1,n-2)]+\theta_1(E_2,n)[D_c(E_1,E_2,n-2)$$
$$-C_c(E_2,E_1,n-2)]+0.5t_{AB}[\eta_2(E_1,n)\theta_3(E_2,n)-\theta_1(E_2,n)\kappa_2(E_1,n)]$$
$$+\kappa_2(E_1,n)\theta_3(E_2,n)[B_c(E_1,E_2,n-1)-B_c(E_2,E_1,n-1)]\},$$

$$Y_u(E_1,E_2,n)=2t_{AB}\{\kappa_2(E_2,n)\theta_2(E_1,n)[B_c(E_1,E_2,n-1)-B_c(E_2,E_1,n-1)]+\theta_3(E_1,n)[C_c(E_1,E_2,n-2)$$
$$-D_c(E_2,E_1,n-2)]+0.5t_{AB}[\kappa_2(E_2,n)\theta_3(E_1,n)-\theta_2(E_1,n)\eta_2(E_2,n)]$$
$$+\theta_3(E_1,n)\eta_2(E_2,n)[A_c(E_1,E_2,n-2)-A_c(E_2,E_1,n-2)]\},$$

$$Z_u(E_1,E_2,n)=2t_{AB}\{\theta_3(E_2,n)\theta_2(E_1,n)[B_c(E_1,E_2,n-1)-B_c(E_2,E_1,n-1)]+\theta_3(E_1,n)\theta_1(E_2,n)[A_c(E_1,E_2,n-2)$$
$$-A_c(E_2,E_1,n-2)]+0.5t_{AB}[\theta_3(E_2,n)\theta_3(E_1,n)-\theta_2(E_1,n)\theta_1(E_2,n)]\},$$

$$A_o(E_1,E_2,n)=2[A_c(E_1,E_2,n-2)-A_c(E_2,E_1,n-2)][B_c(E_2,E_1,n-1)-B_c(E_1,E_2,n-1)],$$

$$B_o(E_1,E_2,n)=2[A_c(E_1,E_2,n-2)-A_c(E_2,E_1,n-2)][C_c(E_2,E_1,n-1)-D_c(E_1,E_2,n-1)],$$

$$C_o(E_1,E_2,n)=2[C_c(E_1,E_2,n-2)-D_c(E_2,E_1,n-2)][C_c(E_2,E_1,n-1)-D_c(E_1,E_2,n-1)],$$

$$D_o(E_1,E_2,n)=2[B_c(E_1,E_2,n-1)-B_c(E_2,E_1,n-1)][C_c(E_2,E_1,n-2)-D_c(E_1,E_2,n-2)],$$

E being either E_1 or E_2. The effective hopping integral, $t(E,n)$, and the effective self-energies of the left and right extreme sites of the renormalized MFS, $E_L(E,n)$ and $E_R(E,n)$, are given by

$$E_R(E,n)=E_R(E,n-2)+t^2(E,n-2)[E-E_R(E,n-1)]/\gamma_F(E,n),$$

$$E_L(E,n)=E_L(E,n-1)+t^2(E,n-1)[E-E_L(E,n-2)]/\gamma_F(E,n),$$

$$t(E,n)=t_{AB}t(E,n-1)t(E,n-2)/\gamma_F(E,n).$$

For the case of free boundary conditions, the Green's functions at the ends of the system are

$$G_{L,L}(E)=[E-E_R(E,n)]/\gamma_G, G_{R,R}(E)=[E-E_L(E,n)]/\gamma_G, \quad G_{L,R}(E)=t(E,n)/\gamma_G,$$

$$\gamma_G=[E-E_L(E,n)][E-E_R(E,n)]-t^2(E,n),$$

and for the case of finite-lead boundary conditions, they are

$$G_{L,L}(E)=\left\{E-E_L(E,n)-\frac{t^2}{E-E_{RP}(E,m)}-\frac{t^2(E,n)}{E-E_R(E,n)-t^2/[E-E_{LP}(E,m)]}\right\}^{-1},$$

$$G_{R,R}(E)=\left\{E-E_R(E,n)-\frac{t^2}{E-E_{LP}(E,m)}-\frac{t^2(E,n)}{E-E_L(E,n)-t^2/[E-E_{RP}(E,m)]}\right\}^{-1},$$

$$G_{L,R}(E)=G_{R,R}(E)t(E,n)/\{E-E_L(E,n)-t^2/[E-E_{RP}(E,m)]\},$$

where m is the generation number of the *periodic* leads built following the Fibonacci procedure, and their effective self-energies and effective hopping are given by

$$E_{LP}(E,m)=E_{LP}(E,m-1)+t_P^2(E,m-1)[E-E_{LP}(E,m-2)]/\gamma_P(E,m),$$

$$E_{RP}(E,m)=E_{RP}(E,m-2)+t_P^2(E,m-2)[E-E_{RP}(E,m-1)]/\gamma_P(E,m),$$

$$t_P(E,m)=t\,t_P(E,m-1)t_P(E,m-2)/\gamma_P(E,m),$$

with

$$\gamma_P(E,m)=[E-E_{RP}(E,m-1)][E-E_{LP}(E,m-2)]-t^2.$$

Finally, the initial conditions for the iterative procedure are

$$t(E,2)=t_{BA},E_L(E,2)=-\alpha,E_R(E,2)=\alpha,$$

$$t(E,3)=t_{AA}t_{BA}/(E-\alpha),E_L(E,3)=-\alpha+t_{BA}^2/(E-\alpha),\quad E_R(E,3)=\alpha+t_{AA}^2/(E-\alpha),$$

$$t_P(E,2)=t,E_{RP}(E,2)=E_{LP}(E,2)=0,$$

$$t_P(E,3)=t^2/E,\quad E_{LP}(E,3)=E_{RP}(E,3)=t_P(E,3),$$

$$A(E_1,E_2,2)=C(E_1,E_2,2)=D(E_1,E_2,2)=I(E_1,E_2,2)=0,$$

$$J(E_1,E_2,2)=K(E_1,E_2,2)=L(E_1,E_2,2)=Z(E_1,E_2,2)=0,$$

$$B(E_1,E_2,2)=2t_{BA}^2,\ F(E_1,E_2,2)=-t_{BA}^2,$$

$$A(E_1,E_2,3)=-[t(E_1,3)-t(E_2,3)]^2t_{BA}^2/t_{AA}^2,$$

$$B(E_1,E_2,3)=4(t^2(E_1,3)+t^2(E_2,3)),\ C(E_1,E_2,3)=-[t(E_1,3)-t(E_2,3)]^2t_{AA}^2/t_{BA}^2,$$

$$D(E_1,E_2,3)=2[t^2(E_1,3)-t^2(E_2,3)]t_{BA}/t_{AA},\ F(E_1,E_2,3)=-[t(E_1,3)+t(E_2,3)]^2,$$

$$I(E_1,E_2,3)=2[t^2(E_2,3)-t^2(E_1,3)]t_{AA}/t_{BA},\ J(E_1,E_2,3)=-t(E_2,3)t_{BA}/t_{AA},$$

$$K(E_1,E_2,3)=2t(E_2,3),\ L(E_1,E_2,3)=-t(E_2,3)t_{AA}/t_{BA},\ Z(E_1,E_2,3)=0,$$

$$A_c(E_1,E_2,2)=B_c(E_1,E_2,2)=C_c(E_1,E_2,2)=0,\ D_c(E_1,E_2,2)=t_{BA},$$

$$A_c(E_1,E_2,3)=t_{BA}^2/(E_1-\alpha),\ B_c(E_1,E_2,3)=t_{AA}^2/(E_2-\alpha),\ C_c(E_1,E_2,3)=0,$$

and

$$D_c(E_1,E_2,3)=t_{AA}t_{BA}/[E_1-\alpha]+t_{AA}t_{BA}/[E_2-\alpha].$$

For the case of the DOS, the renormalization procedure is much simpler, since only a sum of diagonal elements of Green's functions is involved, instead of products of them in the Kubo-Greenwood formula. In this case, we have

$$\mathrm{DOS}(E)=-\frac{1}{\pi}\mathrm{Im}\sum_j G_{j,j}(E^+)=-\frac{1}{\pi}\mathrm{Im}\{D_1(E^+,n)G_{L,L}(E^+)+D_2(E^+,n)G_{R,R}(E^+)+D_3(E^+,n)G_{L,R}(E^+)+D_4(E^+,n)\}, \tag{A1}$$

where

$$D_1(E^+,N)=D_1(E^+,N-1)+\kappa_1^2(E^+,n)D_1(E^+,N-2)+\eta_1^2(E^+,n)D_2(E^+,N-1)+\eta_1(E^+,n)D_3(E^+,N-1),$$

$$D_2(E^+,N)=D_2(E^+,N-2)+\kappa_2^2(E^+,n)D_2(E^+,N-1)+\eta_2^2(E^+,n)D_1(E^+,N-2)+\eta_2(E^+,n)D_3(E^+,N-2),$$

$$D_3(E^+,N)=\kappa_2(E^+,n)D_3(E^+,N-1)+\kappa_1(E^+,n)D_3(E^+,N-2)+2\,\eta_2(E^+,n)\kappa_1(E^+,n)D_1(E^+,N-2)$$
$$+2\,\eta_1(E^+,n)\kappa_2(E^+,n)D_2(E^+,N-1),$$

$$D_4(E^+,N)=D_4(E^+,N-1)+D_4(E^+,N-2)+\theta_1(E^+,n)D_1(E^+,N-2)+\theta_2(E^+,n)D_2(E^+,N-1),$$

and the initial conditions are

$$D_1(E^+,2)=D_2(E^+,2)=1,\ D_3(E^+,2)=D_4(E^+,2)=0,$$

$$D_1(E^+,3)=1+\frac{t_{BA}^2}{(E^+-\alpha)^2},\ D_2(E^+,3)=1+\frac{t_{AA}^2}{(E^+-\alpha)^2},\ D_3(E^+,3)=\frac{2t_{BA}t_{AA}}{(E^+-\alpha)^2},\ D_4(E^+,3)=\frac{1}{E^+-\alpha}.$$

This renormalization procedure is very computationally efficient, however, high order numerical precision should be used.

APPENDIX B: CALCULATION OF THE RENORMALIZATION COEFFICIENTS

In this appendix we explain the procedure to obtain the coefficients in Eq. (6). As an example, the first coefficient, $A(E_1,E_2,n)$, will be calculated with detail.

From Eq. (5) we take one of the three terms and first, we will consider only the summation over j, which is defined as

$$S_c(E_1,E_2,n,k,k+1)\equiv\sum_{j=1}^{N(n)-1} t_{j,j+1}G_{j+1,k}(E_1)G_{k+1,j}(E_2),$$

and it can be written as

$$S_c(E_1,E_2,n,k,k+1)=A_c(E_1,E_2,n)G_{1,k}(E_1)G_{k+1,1}(E_2)+B_c(E_1,E_2,n)G_{N(n),k}(E_1)G_{k+1,N(n)}(E_2)$$
$$+C_c(E_1,E_2,n)G_{1,k}(E_1)G_{k+1,N(n)}(E_2)+D_c(E_1,E_2,n)G_{N(n),k}(E_1)G_{k+1,1}(E_2),$$

where $A_c(E_1,E_2,n),\ldots,D_c(E_1,E_2,n)$ are defined as the coefficients of the products of two Green's functions that satisfy the homogeneous Dyson equation ($[E-H]G=0$). The contributions of its inhomogeneous term are taken into account in the coefficients $J(E_1,E_2,n)$, $K(E_1,E_2,n)$, $L(E_1,E_2,n)$, and $Z(E_1,E_2,n)$.

The construction rule of the Fibonacci sequence, discussed in Sec. II, leads to

$$S_c(E_1,E_2,n,k,k+1)=S_c(E_1,E_2,n-1,k,k+1)+S_c(E_1,E_2,n-2,k,k+1)+t_{AB}G_{N(n-1)+1,k}(E_1)G_{N(n-1),k+1}(E_2).$$

Hence, the coefficients $A_c(E_1,E_2,n),\ldots,D_c(E_1,E_2,n)$ of Appendix A can be obtained by substituting in the last equation the relations

$$G_{N(n-1),h}(E)=\eta_1(E,n)G_{1,h}(E)+\kappa_2(E,n)G_{N(n),h}(E),$$

$$G_{N(n-1)+1,h}(E)=\kappa_1(E,n)G_{1,h}(E)+\eta_2(E,n)G_{N(n),h}(E),$$

where η and κ are defined in Appendix A, and h can be either k or $k+1$.

Now, rewriting Eq. (5) as

$$S(E_1,E_2,n)=\sum_{k=1}^{N(n)-1} t_{k,k+1}[2S_c(E_1,E_2,n,k,k+1)-S_c(E_1,E_2,n,k+1,k)-S_c(E_2,E_1,n,k,k+1)]$$

and taking only the terms of $A_c(E_1,E_2,n)$ in each S_c we obtain

$$
\begin{aligned}
S_A(E_1,E_2,n) \equiv & \sum_{k=1}^{N(n)-1} t_{k,k+1}[2A_c(E_1,E_2,n)G_{1,k}(E_1)G_{k+1,1}(E_2) - A_c(E_1,E_2,n)G_{1,k+1}(E_1)G_{k,1}(E_2) \\
& - A_c(E_2,E_1,n)G_{1,k}(E_1)G_{k+1,1}(E_2)] \\
= & [2A_c(E_1,E_2,n) - A_c(E_2,E_1,n)] \sum_{k=1}^{N(n)-1} t_{k,k+1}G_{1,k}(E_1)G_{k+1,1}(E_2) \\
& - A_c(E_1,E_2,n) \sum_{k=1}^{N(n)-1} t_{k,k+1}G_{1,k+1}(E_1)G_{k,1}(E_2) \\
= & [2A_c(E_1,E_2,n) - A_c(E_2,E_1,n)][A_c(E_2,E_1,n)G_{1,1}(E_1)G_{1,1}(E_2) + \cdots] - A_c(E_1,E_2,n) \\
& \times [A_c(E_1,E_2,n)G_{1,1}(E_1)G_{1,1}(E_2) + \cdots] \\
= & -[A_c(E_1,E_2,n) - A_c(E_2,E_1,n)]^2 G_{1,1}(E_1)G_{1,1}(E_2) + \cdots,
\end{aligned}
$$

where $G_{1,1}(E)$ corresponds to $G_{L,L}(E)$ in Eq. (6), and we have used the fact that the coefficients $A_c(E_1,E_2,n), \ldots, D_c(E_1,E_2,n)$ do not depend on k. Therefore

$$
A(E_1,E_2,n) = -[A_c(E_1,E_2,n) - A_c(E_2,E_1,n)]^2.
$$

The rest of the coefficients can be obtained following a similar procedure.

---

*Permanent address: ESIME-Culhuacan, IPN, Av. Santa Ana 1000, 04430, México D.F., Mexico.

[1] S.-K. Ma, Rev. Mod. Phys. **45**, 589 (1973).
[2] H. Aoki, J. Phys. C **13**, 3369 (1980).
[3] C.E.T. Gonçalves da Silva and B. Koiler, Solid State Commun. **40**, 215 (1981).
[4] Q. Niu and F. Nori, Phys. Rev. Lett. **57**, 2057 (1986).
[5] J.A. Ashraff and R.B. Stinchcombe, Phys. Rev. B **37**, 5723 (1988).
[6] R.A. Barrio and C. Wang, in *Quasicrystal and Incommensurate Structures in Condensed Matter*, edited by M. José-Yacaman *et al.* (World Scientific, Singapore, 1990), p. 448.
[7] D. Walther and R.V. Baltz, Phys. Rev. B **55**, 8852 (1997).
[8] G.G. Naumis and J.L. Aragón, Phys. Rev. B **54**, 15 079 (1996).
[9] A. Sütő, in *Beyond Quasicrystals*, edited by F. Axel and D. Gratias (Les Editions de Physique, France, 1994), p. 483.
[10] K. Machida and M. Fujita, Phys. Rev. B **34**, 7367 (1986).
[11] T. Geisel, R. Ketzmerick, and G. Petschel, Phys. Rev. Lett. **66**, 1651 (1991).
[12] S.N. Evangelou and J.-L. Pichard, Phys. Rev. Lett. **84**, 1643 (2000).
[13] A. Aldea and M. Dulea, Phys. Rev. Lett. **60**, 1672 (1988).
[14] M.E.J. Newman and R.B. Stinchcombe, Phys. Rev. B **43**, 1183 (1991).
[15] D. Mayou, Phys. Rev. Lett. **85**, 1290 (2000).
[16] E. Maciá and F. Domínguez-Adame, Phys. Rev. Lett. **76**, 2957 (1996).
[17] X. Huang and C. Gong, Phys. Rev. B **58**, 739 (1998).
[18] R. Oviedo-Roa, L.A. Pérez, and C. Wang, Phys. Rev. B **62**, 13 805 (2000).
[19] B. Kramer and A. MacKinon, Rep. Prog. Phys. **56**, 1469 (1993).
[20] C. Wang, R. Oviedo-Roa, V. Sánchez, and L.A. Pérez, in *Quasicrystals-Preparation, Properties and Applications*, edited by E. Bellin-Ferré *et al.*, MRS Symposia Proceedings No. 643 (MRS, Pittsburgh, 2001).
[21] R. de Picciotto, H.L. Stormer, L.N. Pfeiffer, K.W. Baldwin, and K.W. West, Nature (London) **411**, 51 (2001).
[22] N. Mott, *Conduction in Non-Crystalline Materials* (Clarendon, Oxford, 1987), p. 25.
[23] E.N. Economou, *Green's Functions in Quantum Physics* (Springer-Verlag, New York, 1983), p. 80.
[24] M. Kohmoto, B. Sutherland, and C. Tang, Phys. Rev. B **35**, 1020 (1987).
[25] C. Wang and R.A. Barrio, Phys. Rev. Lett. **61**, 191 (1988).